Prediction of salt rejection by nanofiltration and reverse osmosis membranes using Spiegler-Kedem model and an optimisation procedure

Noureddine Zouhri[a,*], Mohamed Igouzal[b], Majdouline Larif[a], Mahmoud Hafsi[c], Mohamed Taky[a], Azzedine Elmidaoui[a,*]

[a]*Laboratory of Separation Processes, Department of Chemistry, Faculty of Sciences, Ibn Tofail University, P. O. Box 1246, Kenitra 14000 – Morocco, email: elmidaouiazzedine@hotmail.com (A. Elmidaoui)*
[b]*Interdisciplinary Laboratory for Natural Resources and Environment, Faculty of Sciences, Ibn Tofail University*
[c]*International Institute for Water and Sanitation, National office of Electricity and Potable water (ONEE-IEA), Rabat, Morocco*

ABSTRACT

Many water resources deal with the increasing of sodium and chloride concentrations above the authorized drinking water levels. In order to minimize these concentrations and to achieve a high water quality in the distribution system, membrane processes are becoming a promising technology. In this study, Reverse Osmosis (RO) and Nanofiltration (NF) have been investigated on drinking water of M'rirt city (Morocco). The influence of different operational conditions (applied pressure, recovery rate) on the removal of NaCl and using three NF membranes (NF270*4040, NF90*4040, TR60) and two RO membranes (BW30LE4040, TM710) was studied. The Spiegler–Kedem model was applied to predict the membranes removal process. Model constants are the reflection coefficient and permeability coefficient. They were optimized using the Levenberg-Marquardt algorithm which solves non-linear least-squares problems using an iterative technique. Good agreement between experimental rejection rates and model predicted rejection rates was obtained. Also, both convective and diffusive components of the solute mass transport have been calculated using another form of the basic thermodynamic equations. This allowed having a better understanding of transport phenomena and a better comparison of membranes performances.

Keywords: Reverse osmosis; Nanofiltration; Desalination; Spiegler-Kedem model; Optimization procedure

1. Introduction

RO is a physical process that uses the osmosis phenomenon that is the osmotic pressure difference between the salt water and the pure water to remove the salts from water. RO is a pressure driven membrane process where a feed stream flows under pressure through a semipermeable membrane, separating two aqueous streams, one rich in salt and other poor in salt. Water will pass through the membrane, when the applied pressure is higher than the osmotic pressure, while salt is retained. As a result, a low salt concentration permeate stream is obtained and a concentrated brine remains at the feed side [1].

RO membrane technology has been developed over the past 40 years, being the leading technology for new desalination installations [2]. RO membranes are currently used in a wide range of applications, including brackish/seawater desalination, drinking water treatment and wastewater reuse [3]. It is currently the most important and commonly used desalination technique [4].

Today, cross-linked fully aromatic polyamide is widely regarded as the most effective and reliable material for RO applications. Over the years, research efforts have resulted in tremendous improvements in the performance of these membranes [5].

*Corresponding author.

NF is a membrane operation which allows partial desalination of brackish water and which also has certain selectivity between the different species to be eliminated. If in RO all salts are removed and this requires a step remineralization [6,7]. Development of innovative materials with improved properties is a key issue for the further development of the membrane science and technology. Currently, NF experiencing considerable industrial expansion for the treatment of water and gradually replacing the reserved areas of the RO, in particular for the treatment of brackish water [8–10,18]. NF used two mass transfer mechanisms: forced convection and solubilisation-diffusion [9,19,20], while RO is governed by solubilisation/diffusion.

In NF the passage of the solvent is facilitated by an opening of larger pores accompanied by a higher water load membrane. Therefore, the passage of the salts is higher in NF. The increase in the transfer of salts results in a lowering of the difference in osmotic pressure on either side of the membrane, which also results in lower starting pressure in NF than in RO.

The selectivity differences between ions are more marked in NF because of their high dependence of the operating conditions (transmembrane pressure, recovery rate, salinity, etc.). Generally the technique used for evaluating membranes is the measure of the permeability and rejection of charged and uncharged solutes. However, the selection of a membrane for a given application is far from optimum based on these parameters alone [11].

Moroccan cities situated in the Atlas Mountains are suffering from the increased of salt levels in the drinking water, due to the existence of salt-bearing rocks which contaminate such waters. M'rirt is a small mountain Moroccan city, located at 1113 m above sea level, which recorded a notable increase in salinity of drinking water due to the increase in Na^+ and Cl^- contents that exceeds the World Health Organization (WHO) standards. Drinking water of M'rirt city comes from Oum Errabia River having a mean water conductivity that can achieve 2140 $\mu S \cdot cm^{-1}$.

The aim of this study is to investigate remedial options for the removal of excessive salinity using commercial membranes of RO and NF. An experimental NF and RO pilot was installed at the drinking water treatment plant of M'rirt city, downstream of conventional treatment system and conducted from 2009 to 2011. The experiments were carried out in the pressure range of 6–40 bar. Two complementary approaches will be implemented: (i) determination of hydraulic (water flux) and physico-chemical (ion rejection) characteristics. (ii) the modeling of the matter transfer using Spiegler-Kedem model to assess the convective and diffusional contribution during the transport of Na^+ and Cl^- in the studied membranes.

2. Theoretical background: Spiegler–Kedem model

Membrane performance is measured in terms of salts rejection R(%) and permeate flux, J_v (m·s⁻¹). For dilute aqueous mixtures consisting of water and a solute, the selectivity of a membrane toward the mixture is usually expressed in terms of the observed solute rejection coefficient. This parameter is a measure of a membrane's ability to separate the solute from the feed solution, and is defined, as a percentage, by the equation:

$$R = 100\frac{C_f - C_p}{C_f} = 100\left(1 - \frac{C_p}{C_f}\right) \tag{1}$$

where C_p and C_f are the solute concentration in the permeate and feed solution, respectively.

The Spiegler-Kedem model, based on irreversible thermodynamics, provides a simple framework for description of solute transport in both RO and NF processes. In this model, the membrane is regarded as a "black-box". The Spiegler-Kedem model considers convective coupling of solute and solvent species. For the derivation of the Spiegler-Kedem model, the starting point is the assumption that the water flux (J_v) and the solute flux (J_s) are driven by forces F_v and F_s, respectively. These generalized forces are due to chemical potential gradients across the membrane:

$$J_v = L_{11}F_v + L_{12}F_s \tag{2}$$

$$J_s = L_{21}F_v + L_{22}F_s \tag{3}$$

where L_{ij} are phenomenological coefficients.

The chemical potential gradient is caused by a concentration or pressure gradient. So that the final working equations of the nonlinear Spiegler-Kedem model are:

$$J_v = L_p\,(\Delta P - \sigma\,\Delta\Pi) \tag{4}$$

$$J_s = P_s\,(C_0 - C_p) + (1 - \sigma)\,J_v C_m \tag{5}$$

where ΔP: transmembrane pressure. $\Delta\Pi$: difference in osmotic pressure on either side of the membrane (bar). C_0, C_p, C_m: concentrations respectively in feed, permeate and in the membrane (mg·l⁻¹). L_p: hydraulic permeability of the membrane (l·h⁻¹ bar⁻¹). σ: reflection coefficient (dimensionless). P_s: solute permeability (m·s⁻¹).

We define the product ($\sigma \cdot \Delta\Pi$) as the starting pressure (or called critical pressure, denoted Pc). The reflection coefficient σ is a measure of the relative permeability of a particular membrane to a particular solute. $\sigma = 1$, if the solute is completely excluded and $\sigma = 0$, if the membrane is unselective. Integration of Eqs. (4) and (5) combined with relation (1) and considering the limit conditions of the problem (for $x = 0$, $C_m = C_f$ and for $x = \Delta x$, $C_m = C_p$) lead to relations (6) and (7):

$$R = 1 - \frac{C_p}{C_f} = \frac{\sigma(1 - F)}{1 - \sigma F} \tag{6}$$

$$F = \exp\left(-\frac{(1 - \sigma)J_v}{P_s}\right) \tag{7}$$

where F is a flow parameter (dimensionless); Δx is the membrane thickness (m).

In other hand, in Eq. (5) it is possible to express the solute flux as the sum of a diffusion term and a term of forced convection (advection yet named):

$$J_s = J_{diff} + J_v C_{conv} = C_p J_v \tag{8}$$

where J_{diff} is the solute flux transported by diffusion and C_{conv} the solute concentration in the permeate due to forced convection (here under the influence of a transmembrane hydrostatic force). Then the concentration in the permeate becomes:

$$C_P = \frac{J_{diff}}{J_v} + C_{conv} \qquad (9)$$

Thus by representing the concentration of a solute in the permeate, C_p vs. the inverse of the permeation flux, J_v, a straight line is obtained whose ordinate at the origin is used to find the concentration in the permeate due to the forced convection and slope to determine the diffusion flow. This representation is used to evaluate the weight of these two types of flows encountered in NF [8–10].

2.1. Optimisation procedure

The parameters σ is a measure of the degree of semi-permeability of the membrane, i.e. its ability to pass solvent in preference to solute. It characterizes the imperfection of the membrane [1]. The two transport parameters (σ and P_s) are the main parameter of the model. They were optimized using the Levenberg-Marquardt algorithm which solves non-linear least-squares problems in mathematics and computing using an iterative minimization technique. The Levenberg-Marquardt algorithm is used in many software applications for solving generic curve-fitting problems. The algorithm combines advantages of the steepest descent method (that is, minimization along the direction of the gradient) with the Newton method (that is, using a quadratic model to speed up the process of finding the minimum of a function). Also, Levenberg-Marquardt algorithm finds a solution (parameters estimation) even if it starts very far off the final minimum [12]. The fitted coefficients (σ and P_s) are then said to represent the values of the transport coefficients for the given feed salt composition. Concentration dependence of these coefficients can be assessed by fitting the data for different feed concentrations.

3. Materials and methods

3.1. Characteristics of the feed water

The experiments were conducted on water of M'rirt city. The analytical results of the feed water are shown in Table 1.

3.2. Unit pilot testing

The experiments were performed on an NF/RO pilot plant (E 3039) supplied by TIA Company (Technologies Industrielles Appliquées, France). The operations were conducted in a continuous mode as shown in Fig. 1. The applied pressure over the membrane can be varied from 5 to 70 bar with manual valves.

The pilot plant is equipped with two identical modules operating in series. Each module contains one element. The pressure loss is about 2 bar corresponding to 1 bar of each module. The configuration tested is simple pass in continuous mode.

Table 1
Characteristics of the feed water

Parameters	Feed water
pH	7.74
Conductivity, $\mu S \cdot cm^{-1}$	2140
Temperature,°C	29.0
Suspended maters, ppm	<0.2
Turbidity, NTU	<3
Cl^-, ppm	595.0
TA, °F	0.0
TH, °F	34.65
TAC, °F	34.0
Ca^{2+}, ppm	105.6
Mg^{2+}, ppm	20.05
Na^+, ppm	381
K^+, ppm	3.8
SO_4^{2-}, ppm	60.0
pH_s	7.52
Langelier index	+0.22

Three parameters are monitored during experiments:

The first parameter is the permeation flux deduced from experimental measurements of the receipt volume in a regular time interval given by the equation:

$$J_v = \frac{\Delta V}{\Delta t \cdot S} \qquad (10)$$

where S is the membrane surface.

The second parameter is the recovery rate (Y%) which is defined as:

$$Y = \frac{Q_p}{Q_0} \cdot 100 \qquad (11)$$

where Q_p is permeate flow ($l \cdot h^{-1}$), Q_0 is feed flow ($l \cdot h^{-1}$).

The third parameter is the salt rejection R (%) which is defined by Eq. (6) above.

3.3. Characteristics of the membranes

The two spiral wound modules are equipped with two commercial NF membranes of one type. Table 2 gives the characteristics of the membranes used. After the run, the membranes were cleaned with alkaline and acidic cleaning solutions according to the manufacturer recommendations.

4. Results and discussions

4.1. Effect of the pressure on the permeate flux

In this section, we will study the demineralization of M'rirt water in two recovery rates 30% and 40% in simple pass configuration in continuous mode. Fig. 2 shows the variation of permeate flux as a function of the applied pressure at recovery rates of 30% and 40%.

The analysis of these results show that the permeate flux increases almost linearly with the applied pressure follow-
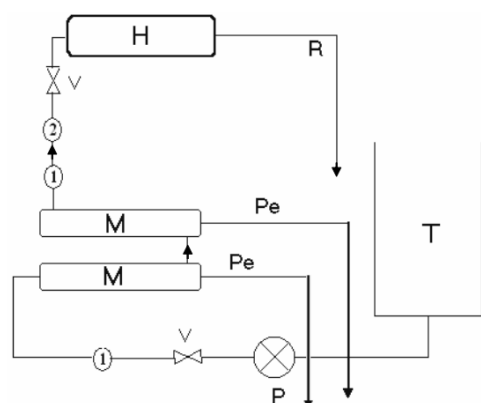
Fig. 1. Schematic diagram and picture of the nanofiltration/reverse osmosis pilot plant. T: tank; P: feed pump; V: pressure regulation valves; M: nanofiltration module; Pe: permeate recirculation; R: retentate recirculation; H: heat exchanger; 1: pressure sensor; 2: temperature sensor.

Table 2
Characteristics of the membranes used

Membrane	Cut-off (Da)	Surface (m²)	Material
NF90*4040	200	7,6	Polyamide
NF270*4040	300	7,6	Polyamide
TR60	400	6,8	Polyamide
BW30LE4040	–	7,6	Polyamide
TM710	–	7,1	Polyamide

ing the Darcy's law. Increasing pressure improves the driving forces and overcome the resistance in the membranes. Also, the permeate flux obtained for the NF membranes are higher than that for the RO membranes. This can be attributed to the nature of the tested membranes, the NF membranes have more opened pores compared to the RO membranes which are denser and tend to be more compact [13]. The permeate flux follows the following order: NF270 > TR60 > NF90 > BW30LE4040 ≈ TM710. On other hand, increasing the recovery rate from 30% to 40% increases the permeate flux, especially for NF membranes.

4.2. Effect of the pressure on the rejection rate

Figs. 3 and 4 represent the variation of the rejection rate of Na^+ and Cl^- as a function of the applied pressure at recovery rates of 30% and 40% respectively.

These figures show that the rejection rate of Na^+ and Cl^- (for Y = 30% and 40%) with RO membranes is higher than that with NF membranes, due to the dense properties of RO membranes. The RO membranes BW30LE4040 and TM710 have rejection for Na^+ and Cl^- nearly equal to the unit and independent of the pressure.

Also, the rejection rate of Na^+ and Cl^- decreases with the increase of the recovery rate from 30% to 40%, especially for NF membranes. These results can be attributed essentially to the increase in the solvent flow [13]. RO membranes remain less influenced by the increase in the recovery rate. For NF membranes, the highest rejection rate is obtained with NF90 which has properties close to RO membranes. In other hand,

the rejection of Na^+ and Cl^- using NF270 increases for pressure between 6 and 10 bar and decreases beyond the pressure of 10 bar. This can be explained by the predominance of ion transport by diffusion at low pressure and by convection at high pressures. Chemical selectivity is always much more important than the physical selectivity to separate ions at low pressure [14]. Also, the difference of rejection between Na^+ and Cl^- ions can be attributed to the difference in their hydration energy [15]. Fig. 5 presents the effect of applied pressure on total dissolved salts (TDS) rejection, for the conversion rates of 30% and 40%. It can be seen from this figure that RO membranes have higher TDS rejection rates, than NF membranes. Also, Fig. 5 confirms that NF90 membrane has properties close to RO membranes for TDS rejection.

4. 3. Application of Spiegler–Kedem model

Experimental data of rejection rates of Na^+ and Cl^- ions as a function of the permeate flux for the five membranes were fitted using Spiegler–Kedem model and Levenberg-Marquardt algorithm to determine optimal values of the reflection coefficient σ and the solute permeability P_s (Figs. 6 and 7). The result shows a good fit of the rejection values for all membranes used and for the two recovery rates (30%, 40%). A summary of the transport parameters (σ, P_s) thus determined for the membranes studied at recovery rates of 30% and 40% is presented in Table 3.

The RO membranes BW30LE4040 and TM710 have high reflection coefficients σ which tends towards the unit in the case of Na^+ and Cl^- ions and for both recovery rates. The two membranes give a complete rejection for the two ions; the ions transport across the two membranes is purely diffusive. The NF90 membrane has a σ value approaching those of RO membranes. As previously mentioned, this membrane has properties close to RO membranes.

The NF membranes (TR60 and NF270) have lower σ values in the case of the two recovery rates due to the low rejection of monovalent ions by NF membranes.

On other hand, Table 3 shows that the parameters P_s and σ are influenced by the recovery rate. Increasing recovery rate from 30% to 40% lead to a decrease in σ value (for Na^+ and Cl^-) especially for NF membranes.
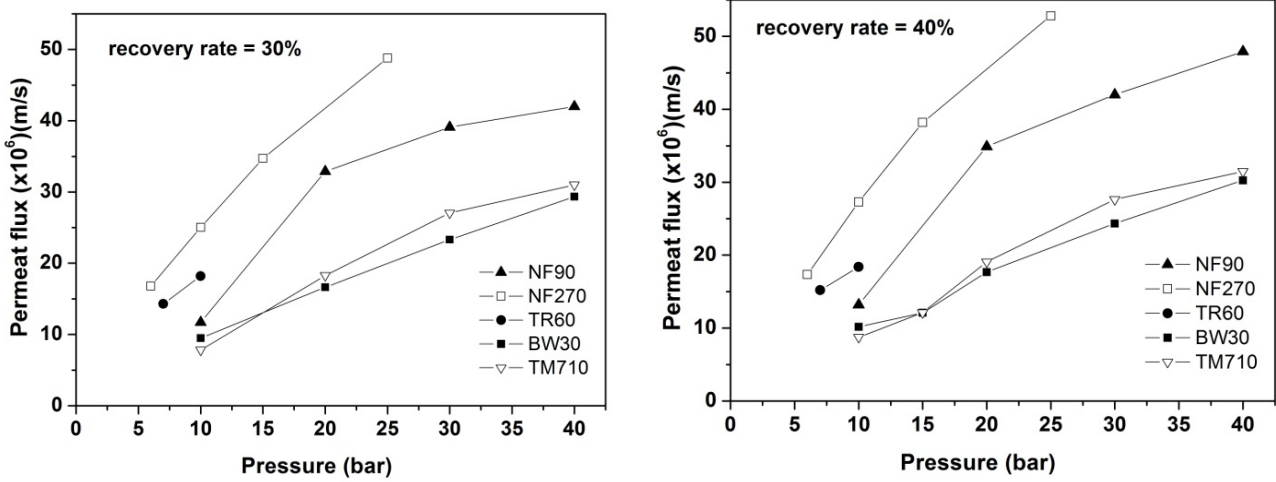
Fig. 2. Variation of permeate flux as a function of the applied pressure for the five membranes for Y = 30% and 40%.
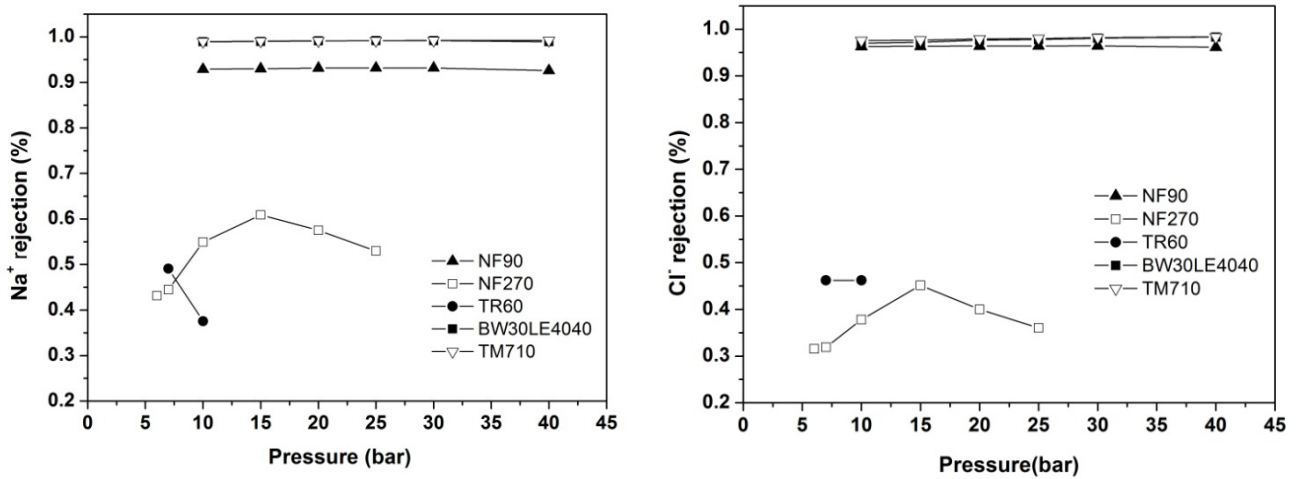
Fig. 3. Variation of rejection rate with pressure for Cl⁻ and Na⁺ for Y = 30% for the five tested membranes.
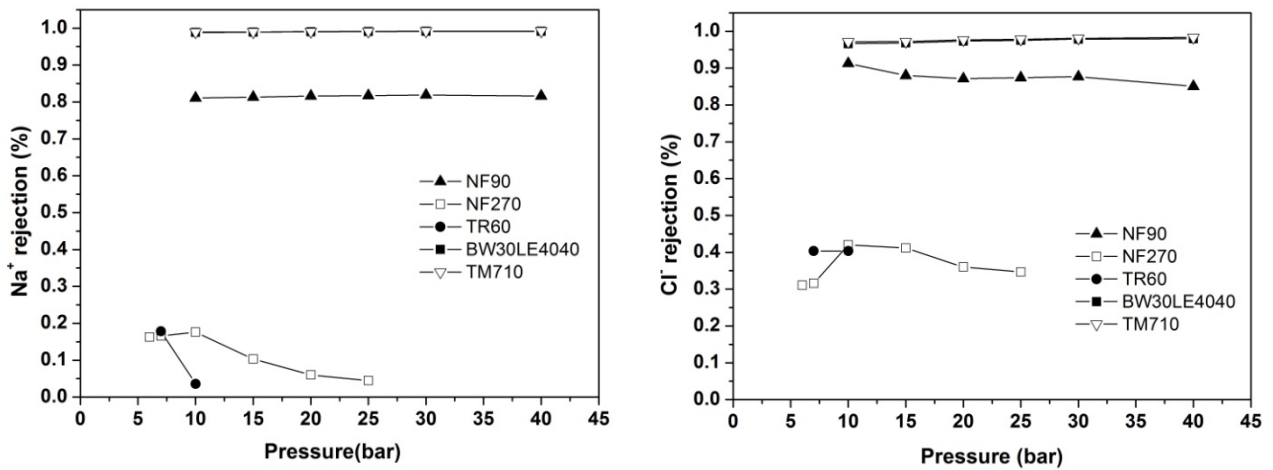
Fig. 4. Variation of rejection rate with pressure for Cl⁻ and Na⁺for Y = 40% for the five tested membranes.
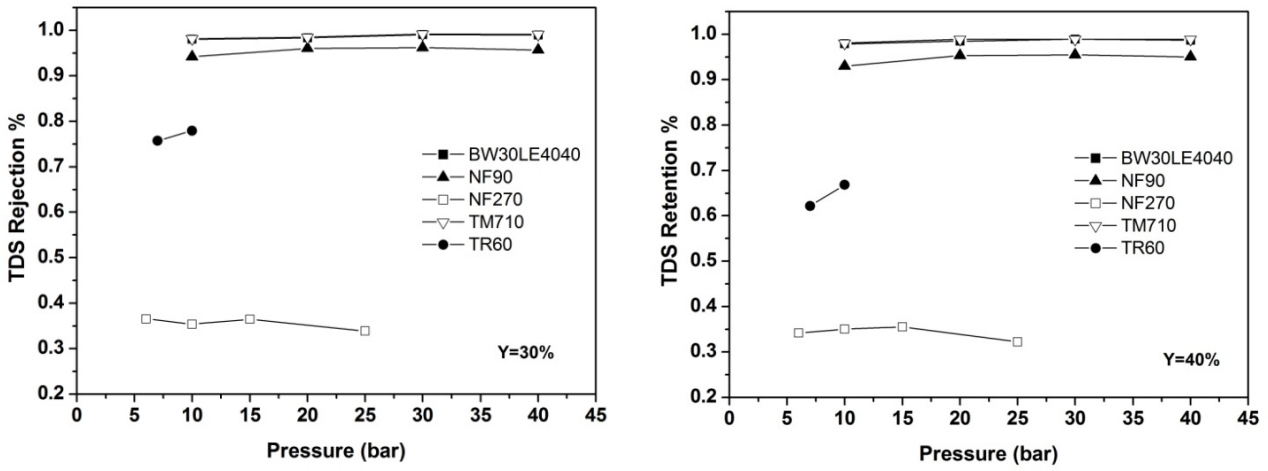
Fig. 5. Variation of TDS retention rate as a function of the applied pressure for Y = 30% and Y = 40%.
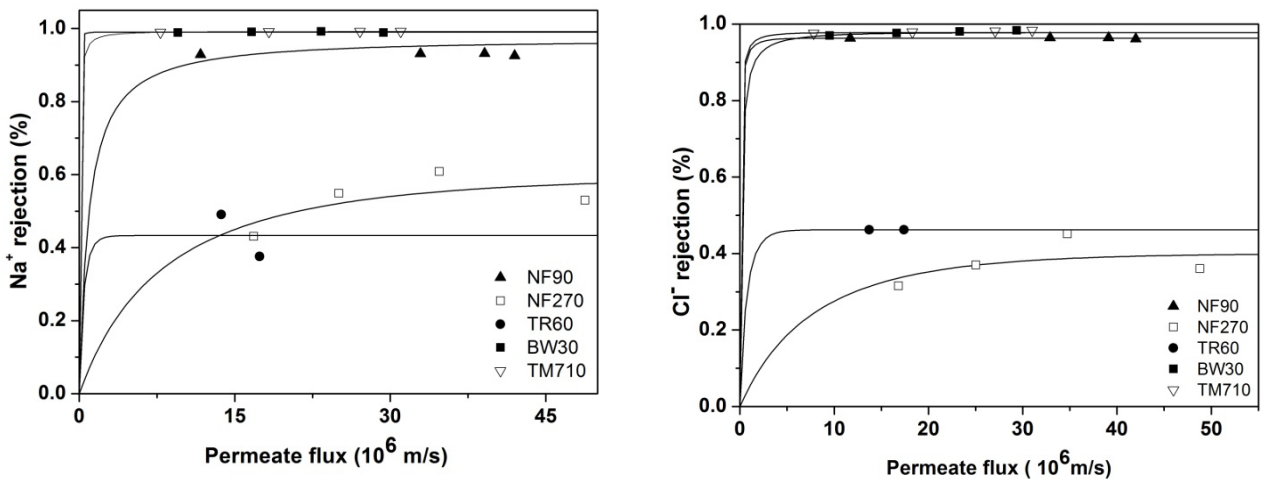
Fig. 6. Effect of permeate flux on rejection of Na$^+$ and Cl$^-$ for the five membranes for Y = 30%.
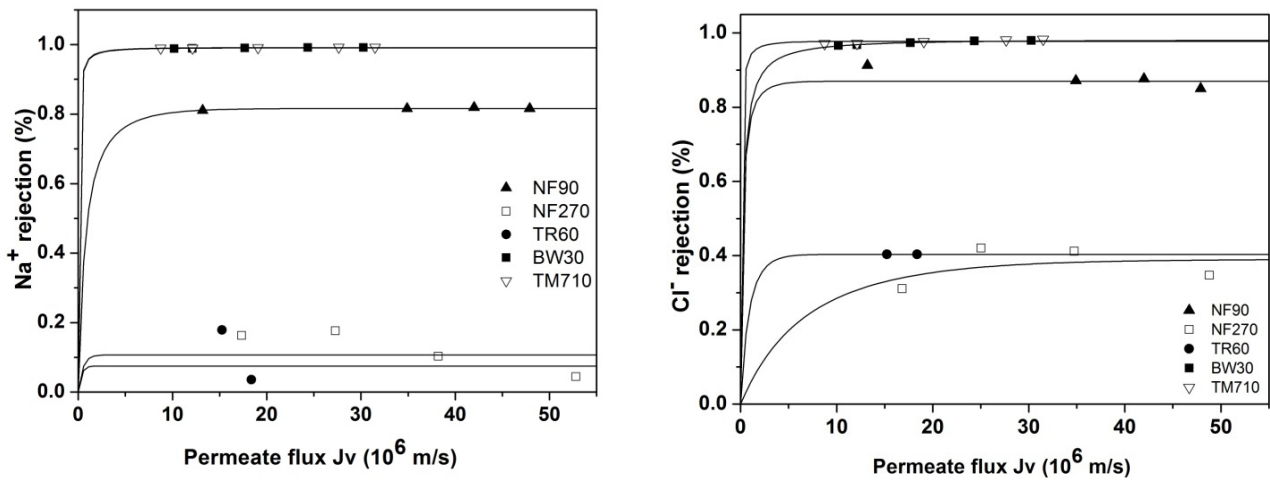
Fig. 7. Effect of permeate flux on rejection of Na$^+$ and Cl$^-$ for the five membranes for Y = 40%.

Table 3
Permeability to solute and reflection coefficient for the five membranes tested at recovery rates of 30% and 40%

Membrane			TR60	NF270	NF90	BW30LE4040	TM710
Y = 30%	Na⁺	σ	0.43	0.59	0.9647	0.99	0.99
		P_s (m·s⁻¹)	3.56·10⁻⁷	7.37·10⁻⁶	8.99·10⁻⁷	4.36·10⁻⁹	3.94·10⁻⁸
	Cl⁻	σ	0.46	0.4	0.96	0.98	0.98
		P_s (m·s⁻¹)	6.04·10⁻⁷	7.11·10⁻⁶	5.47·10⁻⁸	1.50·10⁻⁷	5.17·10⁻⁸
Y = 40%	Na⁺	σ	0.11	0.075	0.8163	0.99	0.99
		P_s (m·s⁻¹)	4.48·10⁻⁷	3.02·10⁻⁷	7.10·10⁻⁷	4.35·10⁻⁸	4.19·10⁻⁸
	Cl⁻	σ	0.40	0.39	0.87	0.98	0.98
		P_s (m·s⁻¹)	7.79·10⁻⁷	6.24·10⁻⁶	2.10⁻⁷	2.47·10⁻⁷	1.35·10⁻⁷
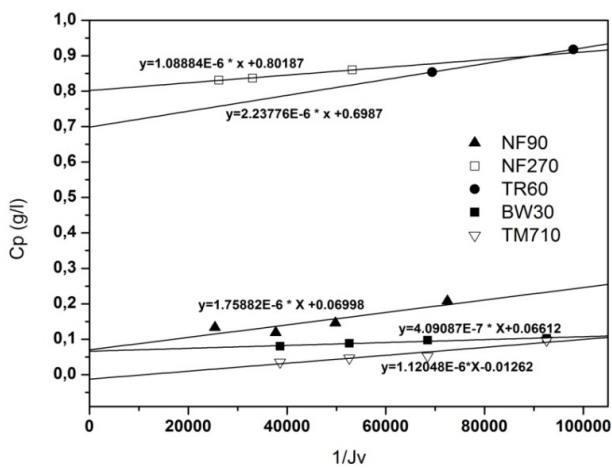
Fig. 8. Evolution of the permeate concentration C_p vs. $1/J_v$ for the five tested membranes for the recovery rate of 30%.

Fig. 9. Evolution of the permeate concentration C_p vs. $1/J_v$ for the five tested membranes for the recovery rate of 40%.

As seen above, Eq. (9) representing C_p vs. the reverse of the permeate flux is applied to experimental results to quantify separately both part of the solutes mass transfer occurring in NF or RO membranes: convection (C_{conv}) and solution/diffusion (J_{diff}). In our case, the solute concentration in the permeate C_p as a function of the reverse of the permeate flux ($1/J_v$) is studied for the five tested membranes for the recovery rates of 30% and 40%. Figs. 8 and 9 reveal a linear relation in conformity with Eq. (9). The intersection point on the ordinate axis of the curve gives the C_{conv} value and the slope gives the value of J_{diff}. Values of C_{conv} and J_{diff} for NF and RO membranes are reported in Table 4.

The C_{conv} values obtained for the RO membranes (BW3040 and TM710) are close to zero. This can be explained by the fact that salt transport through RO membranes occurs only by pure diffusion. For NF membranes TR60 and NF270, nonzero values of C_{conv} and J_{diff} revealed that both modes of transfer (diffusion and convection) occurred together inside this type of membranes. Their magnitude depends on the operating conditions (ionic strength, transmembrane pressure) and also the membrane material [14,16,17]. Hence, the difference between RO and NF is clearly observed and this was consistent with the expected results. From the C_{conv} values for NF membranes, we can notice that NF270 and TR60 membranes are more convective compared to the NF90 membrane. The C_{conv} value of NF90 membrane tends

to zero. The mass transfer properties of the NF90 membrane are very similar to those of RO membranes as mentioned above. On other hand, Table 4 shows that for NF membranes increasing recovery rate from 30% to 40% lead to an increase in diffusive transport (J_{diff}) and convective transport (C_{conv}).

4.4. Statistical analysis and model performance tests

Another way to examine model performance is the plot experimental rejection against predicted rejection. Figs. 10 and 11 show parity plots between calculated and measured rejection rates for Na⁺ and Cl⁻ ions at recovery rates of 30% and 40%, from the five membranes used. In all cases, calculated and experimental rejection rates are very close, as shown by the good approximation to the diagonal. The correlation coefficients are superior to 0,97 which show the perfect fit by the model.

Also, a statistical analysis of residual errors based on the root mean square error (RMSE), the normalized root mean square error (NRMSE) and the Nash-Sutcliffe efficiency (NSE) coefficient was performed.

$$\text{RMSE} = \sqrt{\left[\frac{\sum_{i=1}^{n}\left(x_{\text{meas},i} - x_{\text{pred},i}\right)^2}{N}\right]} \qquad (13)$$

Table 4
Values of C_{conv} and J_{diff} obtained for NF and RO membranes

Recovery rate	Parameter	TR60	NF270	NF90	BW30LE404	TM710
Y = 30%	C_{conv} (g · l⁻¹)	0.6987	0.8018	0.0699	0.0661	≈0
	J_{diff} (kg · m⁻² ·s⁻¹)	$2.237 \cdot 10^{-6}$	$1.088 \cdot 10^{-6}$	$1.758 \cdot 10^{-6}$	$4.0908 \cdot 10^{-7}$	$1.120 \cdot 10^{-6}$
Y = 40%	C_{conv} (g · l⁻¹)	0.7838	0.8869	0.0950	0.0661	≈0
	J_{diff} (kg · m⁻² ·s⁻¹)	$2.409 \cdot 10^{-6}$	$1.185 \cdot 10^{-6}$	$3.768 \cdot 10^{-7}$	$4.090 \cdot 10^{-7}$	$1.120 \cdot 10^{-6}$
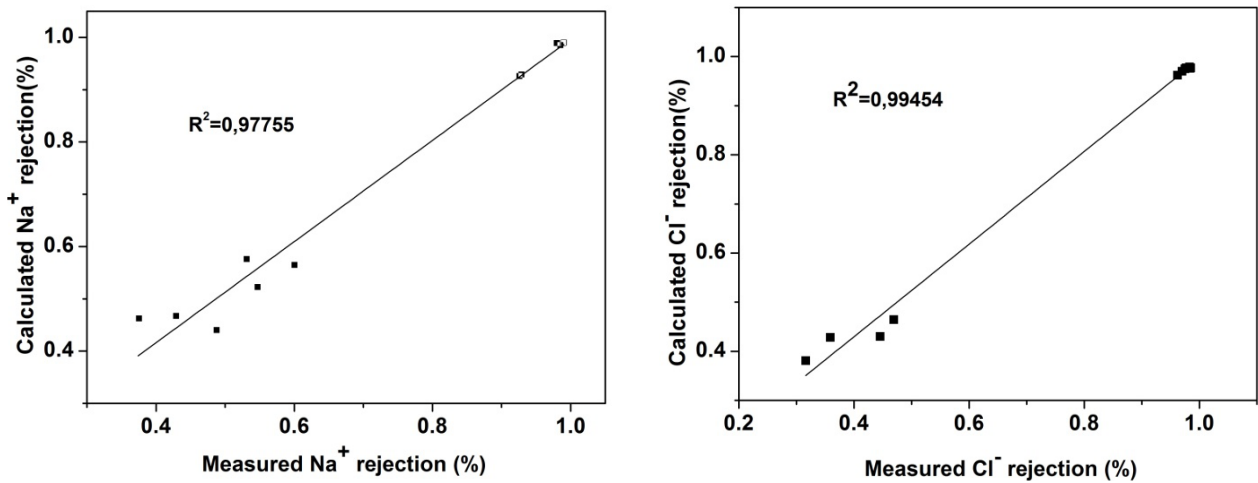
Fig. 10. Parity plots between calculated and measured rejection rates for Na⁺ and Cl⁻ ions for Y = 30%. Each figure includes data from the five membranes tested.
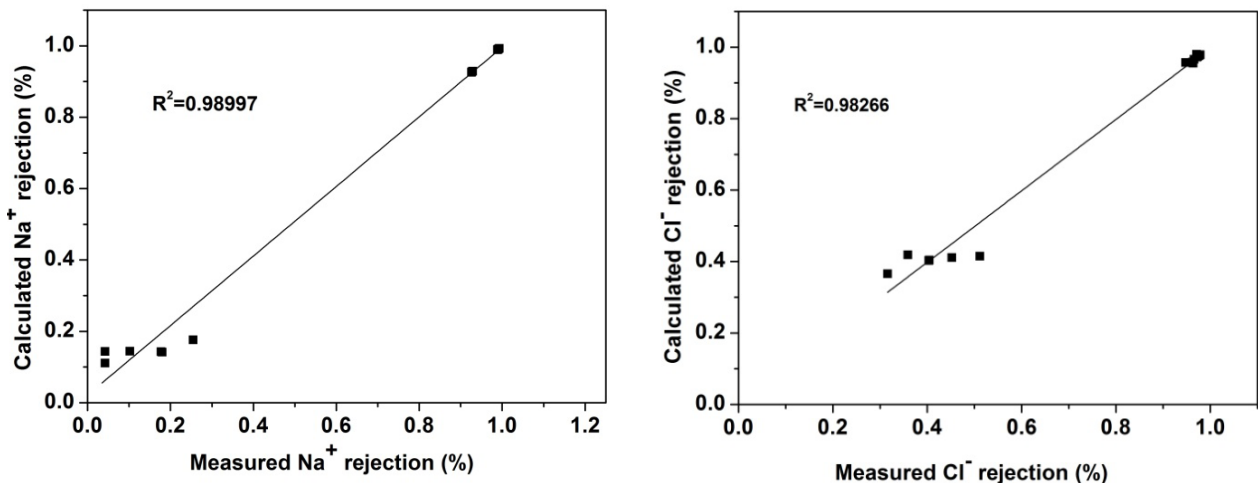
Fig. 11. Parity plot between calculated and measured rejection rates for Na⁺ and Cl⁻ ions for Y = 40%. Each figure includes data from the five membranes tested.

where $x_{meas,i}$: measured rejection rate, $x_{pred,i}$: calculated rejection.

The RMSE is the distance, on average, of a data point from the fitted line, measured along a vertical line. It is directly interpretable in terms of measurement units, and so is a better measure of goodness of fit than the correlation coefficient.

$$NRMSE = \frac{RMSE}{\overline{x}_{meas}} \tag{14}$$

where $\overline{x}_{meas}$: mean measured rejection rate.

The normalized root mean square error (NRMSE) represents a non-dimensional form of the RMSE. A lower value of NRMSE indicates less residual variance.

Table 5
Results of the statistical analysis

Statistical	Parameter	RMSE (%)	NRMSE (–)	NSE (–)
Y = 30%	Na$^+$	0,029	0,036	0,98
	Cl$^-$	0,024	0,029	0,99
Y = 40%	Na$^+$	0,036	0,052	0,99
	Cl$^-$	0.030	0.038	0.97

$$NSC = 1 - \left[\frac{\sum_{i=1}^{n} \left(x_{meas,i} - x_{pred,i} \right)^2}{\sum_{i=1}^{n} \left(x_{meas,i} - \overline{x}_{meas} \right)^2} \right] \tag{15}$$

The Nash-Sutcliffe efficiency (NSE) is a normalized statistic that determines the relative magnitude of the residual variance (noise) compared to the measured data variance (information). It informs on how well the plot of observed vs. simulated data fits the 1:1 line.

Table 5 shows the results of the statistical analysis. The RMES coefficient obtained have a small value, the function is small than unity and the NSE coefficient is very near to 1. This result demonstrates the good performance of the model and the optimization procedure.

5. Conclusion

In this study, RO and NF have been investigated on drinking water of M'rirt city (Morocco). Comparison of the performances (rejection rate) of three commercial NF membranes and two commercial RO membranes in continuous mode was carried out in the removal of monovalent ions (Na$^+$ and Cl$^-$). Rejection exceed 90% for RO membranes, 80% for NF90 membrane and depend on the applied pressure for NF270. Comparison of the experimental results to the Spieegler-Kedem model predictions shows a good agreement, as indicated by the parity plot and the statistical analysis. This result demonstrates the good performance of the model and the Levenberg-Marquardt optimization algorithm. In a second modeling approach, the experimental results of permeate flux and the rejection rate are represented in another way to quantify the contribution of convective and/or diffusion in solute transfer. We obtained that both transfer modes (convection and diffusion) occur for the NF membranes. For NF90*4040 and RO membranes, solute transport is essentially diffusional.

Acknowledgements

Symbols

C_f (kg/m^3) — Solute concentration in the feed stream
C_m (kg/m^3) — Solute concentration in the membrane
C_p (kg/m^3) — Solute concentration in the permeate stream
R^2 — Correlation coefficient
F — Dimensionless parameter of Spiegler-Kedem model
FW — Feed water
J_v (m3/m^2 s) — Permeate flux
J_s (kg/m2 s) — Solute flux
J_w (kg/m2 s) — Water flux
L_p (m/s) — Solvent permeability constant
NSE — Nash-Sutcliffe efficiency
NRMSE — Normalized root mean square error
P (Pa) — Operation pressure
P_s (m/s) — Solute permeability constant
R (%) — Membrane rejection
RMSE — Root mean square error
TH — Total hardness
T (°C) — Temperature
σ — Reflection coefficient
x (m) — Distance across the membrane
ΔP (Pa) — Hydraulic pressure applied across the membrane
Δx (m) — Membrane thickness
$\Delta \Pi$ (Pa) — Difference in the osmotic pressure of the solutions on the feed and permeate side of the membrane

References

[1] B.L. Pangarkar, G.M. Sane, M. Guddad, Reverse osmosis and membrane distillation for desalination of groundwater: a review. International Scholarly Research Network, 2011, pp. 1–9.

[2] A. Pérez-González, R. Ibáñez, P. Gómez, A.M. Urtiaga, I. Ortiz, J.A. Irabien, Nanofiltration separation of polyvalent and monovalent anions in desalination brines, J. Membr. Sci., 473 (2015) 16–27.

[3] L. Eunsu, L. Sangyoup, H. Seungkwan, A new approach to the characterization of reverse osmosis membrane by dynamic hysteresis, Desal. Water Treat., 18 (2010) 257–263.

[4] A. Rodríguez-Calvo, G.A. Silva-Castro, F. Osorio, J.G. López, C. Calvo, Reverse osmosis seawater desalination: current status of membrane systems, Desal. Water Treat., 56 (2015) 849–861.

[5] J.M. Gohila, A.K. Suresh, Development of high flux thin-film composite membrane for water desalination: a statistical study using response surface methodology, Desal. Water Treat., 52 (2014) 5219–5228.

[6] M. Zairi, Evaluation des performances d'une station de dessalement par osmose inverse, TSM, Génie urbain, Génie rural, 4 (2002) 50–58.

[7] M. Pontié, O. Sarr, M. Rumeau, Evaluation des possibilités de dessalement d'une eau saumâtre par osmose inverse et par nanofiltration, L'eau, l'industrie, les nuisances, 210 (1998) 57–63.

[8] H. Dach, Comparaison des opérations de nanofiltration et d'osmose inverse pour le dessalement sélectif des eaux saumâtres : de l'échelle du laboratoire au pilote industriel, PhD thesis, 2008, 192 p.

[9] M. Pontié, H. Dach, J. Leparc, M. Hafsi, A. Lhassani, Novel approach combining physico-chemical characterizations and mass transfer modelling of nanofiltration and low pressure reverse osmosis membranes for brackish water desalination intensification, Desalination, 221 (2008) 174–191.

[10] M. Pontié, C.K. Diawara, A. Lhassani, H. Dach, M. Rumeau, H. Buisson, J.C. Schrotter, Water defluoridation processes: A review, Application: nanofiltration for future large-scale pilot plants, 2 (2006) 49–80.

[11] M. Pontié, C. Diawara, A. Gonidec, L. Stricot, A. Lhassani, H. Dach, P. Bourseau, P. Jaouen, Défluoruration des eaux par nanofiltration à grande échelle: Thiadiaye (Sénégal), une première mondiale. Journées Informations Eaux, 2010, Poitiers, France.

[12] K. Levenberg, A method for the solution of certain non-linear problems in least squares, Quart. Appl. Math., 2 (1944) 164–168.

[13] F. ElAzhar, R. El Habbani, M. Elazhar, M. Hafsi, A. Elmidaoui, Comparison of the performances of two commercial membranes in hardness removal from underground water using nanofiltration membranes, Int. J. Adv. Chem., 1 (2013) 21–30.

[14] D. Szaniawska, H.G. Spencer, Non-equilibrium thermodynamics analysis of the transport properties of formed-inplace Zr(IV) hydrous oxide–PAA membranes. II. NaCl–water solutions, Desalination, 101 (1995) 31.

[15] F. El Azhar, N. Zouhri, S. Aithabzize, M. Taky, A. Elmidaoui, Study of Atlantic seawater desalination by reverse osmosis using a pilot plant, Phys. Chem. News, 58 (2011) 20–24.

[16] C.K. Diawara, M. Sidy Lô, M. Rumeau, M. Pontie, O. Sarr, A phenomenological mass transfer approach in nanofiltration of halide ions for a selective defluorination of brackish drinking water, J. Membr. Sci., 219 (2003) 103–112.

[17] R.E. Lebrun, Y. Xu, Dynamic characterization of nanofiltration and reverse osmosis membranes, Sep. Sci. Technol., 34 (1999) 1629–1641.

[18] F. Elazhar, M. Tahaikt, A. Achatei, F. Elmidaoui, M. Taky, F. El Hannouni, I. Laaziz, S. Jariri, M. El Amrani, A. Elmidaoui, Economical evaluation of the fluoride removal by nanofiltration, Desalination, 249 (2009) 154–157.

[19] M. Tahaikta, A. AitHaddou, R. El Habbani , Z. Amor, F. El hannouni, M. Taky, M. Kharif, A. Boughriba, M. Hafsi, A. Elmidaoui, Comparison of the performances of three commercial membranes in fluoride removal by nanofiltration. Continuous operations, Desalination, 225 (2008) 209–219.

[20] M. Tahaikt, R. El Habbani, A. AitHaddou, I. Achary, Z. Amor, M. Taky, A. Alami, A. Boughriba, M. Hafsi, A. Elmidaoui, Fluoride removal from groundwater by nanofiltration, Desalination, 212 (2007) 46–53.